applied sciences

MDPI

Article

Multiscale Fracture Characteristics of Coal and Their Influence on Fracture Propagation

Jie Bai [1,2], Haige Wang [2], Guangcong Ren [2] and Yan Qiao [2,*]

[1] Research Institute of Petroleum Exploration & Development, Beijing 100083, China; baij9266@126.com
[2] CNPC Engineering Technology R&D Company Limited, Beijing 102206, China; wanghaigedri@cnpc.com.cn (H.W.); renguangcongdri@cnpc.com.cn (G.R.)
* Correspondence: qiaoy103@163.com

Abstract

The complex natural fracture system in coalbed methane reservoirs plays a critical role in hydraulic fracture propagation. This study investigates coal specimens collected from the subsurface of the Ordos Basin (North China). By integrating CT scanning, X-ray diffraction, nanoindentation, and compression tests, the authors systematically characterized the natural fracture development, mineral composition, and mechanical properties of the coal. Based on these data, a numerical model of coal formation was established using the discrete fracture network (DFN) method to evaluate the influence of natural fracture characteristics on hydraulic fracture propagation. Finally, based on a field fracturing case, recommendations for fracturing treatment design are proposed.

Keywords: coal; cleat; multiscale fractures; hydraulic fracturing

1. Introduction

Coalbed methane (CBM) development has undergone a notable evolution,, extending from shallow (<1000 m) to deep (>2000 m) formations, as exemplified by successful commercial production in regions such as Ordos Basin, China [1–3]. Current development strategies primarily rely on horizontal wells combined with large-scale hydraulic fracturing to enhance single-well productivity. Therefore, a thorough understanding of fracture propagation mechanisms in coal reservoirs is essential for improving efficiency and reducing development costs [4].

As an unconventional reservoir, coal is characterized by a complex natural fracture system, where the geometry and distribution of cleats significantly influence the initiation and propagation of hydraulic fractures [5–8]. Natural fractures in coal are typically distributed in a network consisting of high-angle face cleats and butt cleats, forming an orthogonal system [9,10]. These pre-existing fractures may either serve as pathways for hydraulic fracture extension or lead to substantial fluid loss, thereby affecting overall stimulation efficiency [11–15]. Consequently, investigating the multiscale fracture characteristics of coal and their influence on hydraulic fracture behavior is of both theoretical and practical significance for optimizing CBM development and maximizing stimulated reservoir volume (SRV).

Currently, scholars have conducted extensive research on the fracture propagation characteristics of coal. Tan, Huang, et al. investigated the effects of horizontal stress difference, elastic modulus, and fracturing fluid viscosity on hydraulic fracture propagation through physical simulation experiments [16–19]. Li, Teufel, et al. found that whether a

Check for updates

Academic Editor: Ricardo Castedo Ruiz

Received: 25 February 2026
Revised: 18 March 2026
Accepted: 24 March 2026
Published: 26 March 2026

Copyright: © 2026 by the authors. Licensee MDPI, Basel, Switzerland. This article is an open access article distributed under the terms and conditions of the Creative Commons Attribution (CC BY) license.

fracture can cross coal bedding planes is influenced by the shear strength and frictional properties of these planes. Meanwhile, bedding planes may induce fracture branching or arrest propagation, thereby promoting the formation of complex fracture networks [20,21]. Wu et al. studied the impact of cluster spacing on fracture propagation and suggested that excessively close spacing leads to inter-cluster interference [22]. Liu et al. observed that by varying the injection rate during fracturing, multiple points can be simultaneously initiated, facilitating the formation of fracture networks [23]. Yang et al. conducted pulse fracturing tests on coal and found that cyclic loading, achieved through rapid changes in treatment pressure and frequency, resulted in more complex fractures [24]. CT scanning has become a widely used method for characterizing natural fractures in rock. Wang K and Xu, et al. [25,26] employed CT scanning to reconstruct digital cores of coal specimens and conducted numerical simulations of uniaxial compression tests to analyze the influence of cleats on coal strength. Similarly, Ju et al. [27] performed CT scanning on post-failure coal specimens to investigate fracture propagation during loading.

Numerical simulation serves as a key method for investigating hydraulic fracturing mechanisms. Tian, Xu, et al. performed numerical simulations of hydraulic fracturing in coal reservoirs using the finite element method, exploring the effects of injection rate, treatment scale, and fluid viscosity on fracture propagation in terms of height and length [25–27]. Wang, Xia, et al. discovered that the stress shadow generated during hydraulic fracturing significantly influences fracture propagation, potentially causing fracture deflection or growth arrest [28,29]. Conversely, excessive fracture spacing may lead to unstimulated zones, reducing stimulation efficiency [30,31]. Li et al. simulated fracture propagation during vertical well fracturing in coal reservoirs and concluded that increasing fluid viscosity and injection rate promotes uniform propagation of multi-layer fractures [20,32,33].

However, existing research on fracture propagation in coal lacks systematic investigation into the intrinsic properties of cleats, such as density, orientation, and size, and their influence on fracture propagation. There is a notable absence of multi-scale analyses [34–38] that integrate observations from the micro to macro scale and combine experimental with simulation approaches. Consequently, numerical models often fail to realistically represent the morphology of cleat systems. To address this, the present study employs FracMan 7.8 software to develop a reservoir model based on a 3D stochastic fracture modeling approach, which more accurately captures the characteristics of coal.

This study integrates microscale experiments (micro-CT imaging and nanoscale mechanical testing), core-scale mechanical experiments, and field-scale numerical simulations of hydraulic fracturing to systematically elucidate the multiscale characteristics of natural fractures in coal and their governing mechanisms on hydraulic fracture propagation. The nanoscale mechanical differences between organic matter and quartz in coal were quantified and linked to macroscopic mechanical behavior. The nonlinear effects of natural fracture density, orientation, and size on hydraulic fracture length and stimulated volume were quantitatively evaluated, and key controlling parameters were identified. Based on the results, it is concluded that fracture propagation in coal is jointly governed by the properties of its microscopic components and the multiscale natural fracture network.

2. Materials and Methods

Deep coalbed methane reservoirs are typically buried at depths exceeding 1500 m. In this study, experimental investigations were conducted on core specimens obtained from a depth of 1500 m in the eastern margin of the Ordos Basin.

2.1. CT Scanning Test

To investigate the spatial distribution characteristics of cleats in coal, CT scanning was performed on two coal specimens in this study. During CT scanning, coal specimens were wrapped in thin foam to prevent artifacts caused by shaking. Each scan lasted 45 min, achieving a spatial resolution of 5.0 μm. A high-sensitivity detector was employed during CT scanning to obtain clear CT images. To clarify the fracture characteristics of the rock mass, a spherical coordinate system was introduced for the evaluation of rock fractures (Figure 1).

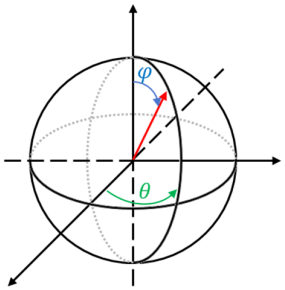


Figure 1. Spherical coordinate system.

2.2. XRD Test

Mineral composition is a key factor influencing the mechanical properties of rocks. Specimens measuring 5 × 5 × 5 mm were cut from the surface of two coal specimens for XRD analysis. Each group of rock specimens was ground into a powder with particle diameters less than 0.08 mm. The powder was then placed in an X-ray diffractometer to obtain diffraction patterns. Based on the diffraction signal characteristics of different minerals, the types and contents of minerals in the coal were identified [39].

2.3. Nanoindentation Test

In this study, nanoindentation tests were conducted on coal specimens retrieved from a depth of 1500 m using the TI Premier nanoindentation system (Bruker Corporation, Billerica, MA, USA). The small specimen size required for this technique helps mitigate the challenges associated with acquiring downhole coal specimens and the limited number of available specimens. Tests were performed on one coal specimen. Owing to the uneven surface, loose texture, and the presence of numerous micro-fractures in the coal, multiple preparation steps were necessary to achieve the surface smoothness required for testing [40]. The specimen preparation procedure is illustrated in Figure 2: (1) wire cutting was used to obtain flat rock specimens, which were then divided into small fragments; (2) the fragments were embedded in epoxy resin and allowed to solidify before demolding; (3) the solidified specimens were roughly polished using a polishing machine; (4) fine sandpaper was employed to polish the specimen surface until a mirror finish was achieved.

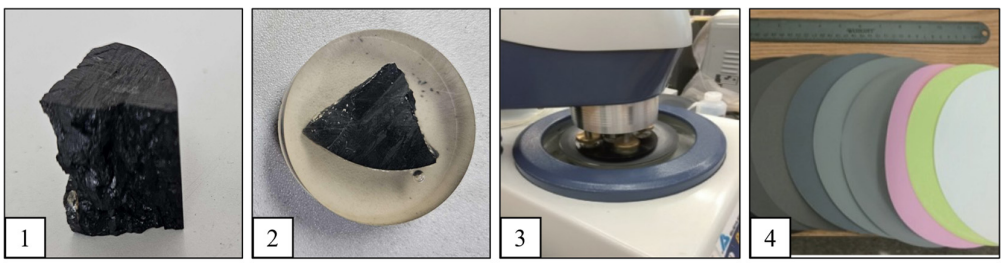


Figure 2. Nanoindentation specimen preparation process.

Given the inherently low hardness of coal, the maximum load during indentation tests was consequently reduced. A load of 8 mN was set as the termination signal. The test procedure for each indentation point included three stages: loading, holding, and unloading, with durations of 5 s, 2 s, and 5 s, respectively. Indentation points were arranged in a 4 × 5 array with a spacing of 50 μm (Figure 3).

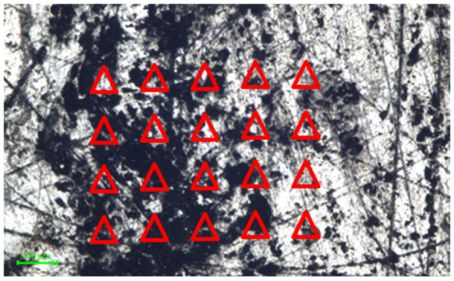


Figure 3. Indentation array. Scale bar: 100 μm.

After the test, the elastic modulus of the tested material was calculated using the classical method proposed by Oliver and Pharr [41] for determining micromechanical parameters. The calculation formula is as follows:

$$E_r = \frac{\sqrt{\pi}}{2\beta}\frac{S}{\sqrt{A}} \quad (1)$$

where E_r is the reduced elastic modulus; A is the projected contact area between the indenter and the material (μm^2); β is the indenter correction factor, which is 1.034 for the indenter used in this study; and S is the slope of the upper part of the unloading curve.

2.4. Uniaxial/Triaxial Compression Test

Compression tests in this study utilized coal specimens taken from a depth of 1500 m in the Ordos Basin. Wire cutting technology was used during specimen preparation to prevent water-induced damage to the coal. Due to the abundant organic matter from lignocellulosic plant tissues during coalification, coal exhibits low strength, well-developed cleats, and a complex natural fracture network. Conventional standard core specimens (diameter 25 mm, height 50 mm) cannot accurately reflect the influence of cleats on coal strength. Therefore, the coal specimens used in these tests had dimensions of 50 mm diameter and 100 mm height (Figure 4a), exhibiting greater randomness in cleat spatial distribution.



(**a**) (**b**)

Figure 4. Test materials and equipment. (**a**) Coal specimen; (**b**) MTS rock testing machine.

Uniaxial compression tests and triaxial compression tests under a confining pressure of 2 MPa were conducted on two sets of coal specimens (Table 1). Although the in situ stress at the target reservoir depth is higher than 2 MPa, the purpose of this experiment

is to compare the differences in the mechanical response of coal under conditions with and without confining pressure, and to obtain basic strength parameters (cohesion and internal friction angle) for numerical model calibration. The test results obtained under low confining pressure are sufficient to meet the requirements for establishing the Mohr–Coulomb strength envelope. Considering the well-developed fractures and loose structure of the specimens, a displacement-controlled loading mode was adopted on the MTS rock testing system (Figure 4b). The axial loading rates of two rock specimens were both 0.002 mm/s.

Table 1. Compression test parameter.

No.	Specimen Size (mm)	Loading Method
Coal C-2	Φ50 × 100	2 MPa Confining Pressure
Coal C-4	Φ50 × 100	Uniaxial

2.5. Hydraulic Fracturing Numerical Simulation

Small-scale fracture networks cannot fully replicate the actual conditions encountered during hydraulic fracturing. This study established a 3D numerical model of fractured coal reservoirs using FracMan software and DFN method. The model aims to investigate the influence of specific fracture attributes on propagation of hydraulic fracture.

The primary development target for deep coalbed methane in the current study area is at a depth of 2000 m, where the stress regime is characterized as normal faulting. The in situ stress values in the numerical model of this study are established based on this background. The maximum horizontal principal stress is oriented north–south with a magnitude of 42 MPa. The minimum horizontal principal stress is 36 MPa, and the vertical stress is 48 MPa.

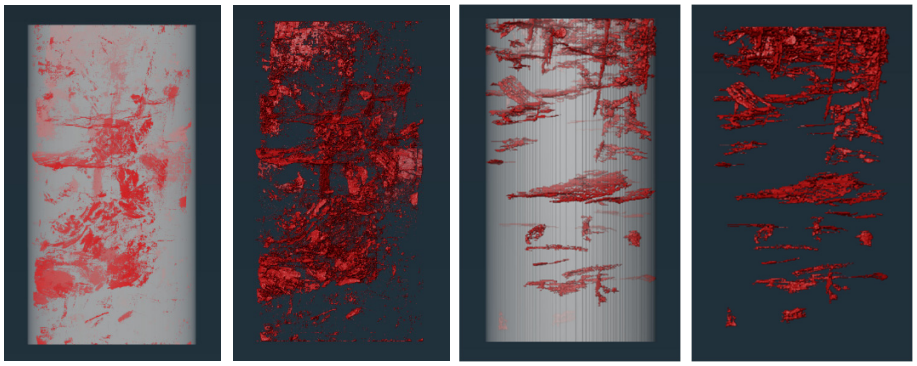
In the hydraulic fracturing simulation, the cleat system in the coal formation was set as high-angle fractures, with butt cleats orthogonal to face cleats [1]. The elastic modulus, Poisson's ratio, cohesion, and friction angle of the reservoir were obtained based on the experimental results of this study.

The simulation considered a horizontal well with three-stage fracturing, three clusters per stage, a stage length of 50 m, and a cluster spacing of 20 m. The treatment scale was set at 2500 m^3 per stage with a pumping rate of 18 m^3/min. These fracturing treatment parameters are representative of those currently used in deep coalbed methane development.

3. Results

3.1. Natural Fracture Development Characteristics

CT scanning revealed the natural fracture distribution in the rock specimens. Three-dimensional visualizations of the scanned coal specimens showed a distinct and complex cleat system (Figure 5). The CT scan results are shown in Table 2. Specimen C-1 has a fractal dimension of 2.14, a porosity of 2.96%, and an average length ranging from 1.18 to 1.37 mm. Specimen C-4 has a fractal dimension of 2.21, a porosity of 2.73%, and an average length ranging from 6.44 to 8.25 mm. As shown in Figure 5, two sets of cleats exist in the core, oriented parallel and perpendicular to the specimen axis.



(a) (b)

Figure 5. CT scan images of coal specimens. (**a**) Coal specimen C-2; (**b**) Coal specimen C-4.

Table 2. Cleat development characteristics in coal specimens.

Core No.	φ			θ	
	Angle Range/°	Fracture Count/cm^3	Avg Length/mm	Angle Range/°	Fracture Count/cm^3
C-2	(0, 20)	1.67	1.29	(−180, 90)	3.34
	(20, 40)	3.23	1.18	(−90, 0)	4.41
	(40, 60)	3.74	1.21	(0, 90)	3.90
	(60, 80)	4.74	1.28	(90, 180)	5.05
	(80, 90)	3.31	1.37		
C-4	(0, 20)	0.3	7.05	(−180, 90)	0.7
	(20, 40)	0.4	7.16	(−90, 0)	0.3
	(40, 60)	0.5	6.44	(0, 90)	1.3
	(60, 80)	0.9	6.63	(90, 180)	0.7
	(80, 90)	0.9	8.25		

3.2. Mineral Composition

X-ray diffraction analysis was used to determine the mineral composition and contents of the coal. According to the mineral content Table 3, the coal primarily consisted of quartz and organic matter, with organic matter constituting approximately 80% of its mass.

Table 3. Mineral content percentage.

No.	Quartz	Plagioclase	Organic Matter	Dolomite	Calcite	Pyrite	Kaolinite	Illite
C-1	12.9%	0	87.1%	0	0	0	0	0
C-4	27.2%	0	72.8%	0	0	0	0	0

3.3. Micromechanical Properties

Nanoindentation tests were performed on smoothly polished coal specimens, involving loading, load holding, and unloading, yielding 20 sets of load-penetration curves (Figure 6). The curves indicated that the nanoindenter penetrated quartz twice and organic matter 18 times, suggesting a quartz content of approximately 10% in the tested area. Under the same load, the penetration depth in quartz was much smaller than in organic matter, and the indentation curve was steeper, reflecting the significantly higher hardness and strength of quartz compared to organic matter. The indentation curves for organic matter were more dispersed, with penetration depths ranging from 900 to 1600 nm, indicating the complex and highly discrete nature of the organic matter components in coal.

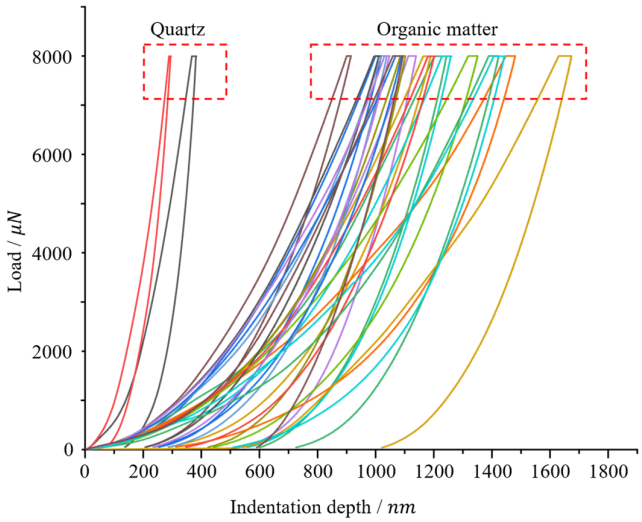


Figure 6. Coal indentation load-indentation depth curves.

Based on the load-indentation depth curves, the elastic modulus of organic matter in coal was calculated to range from 2.5 GPa to 5.67 GPa, with an average of 4.15 GPa. In contrast, quartz exhibited a much higher elastic modulus, varying between 95.60 GPa and 100.20 GPa and averaging 97.90 GPa.

The relationship between mineral elastic modulus and penetration depth showed a strong linear correlation. A greater penetration depth corresponded to a smaller elastic modulus (Figure 7).

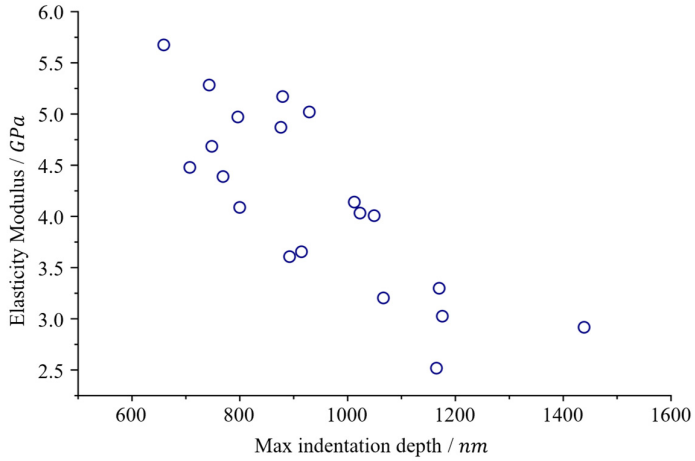


Figure 7. Relationship between indentation depth and elastic modulus for coal.

3.4. Rock Strength and Elastic Parameters

Uniaxial compression and triaxial compression tests (confining pressure 2 MPa) were conducted on the coal specimens. Under uniaxial loading, the failure load of the coal specimen was 15.20 MPa, with an elastic modulus of 3.99 GPa and Poisson's ratio of 0.33. Under triaxial loading with 2 MPa confining pressure, the failure load was 37.71 MPa, with an elastic modulus of 4.85 GPa and Poisson's ratio of 0.31. Based on the stress–strain curves (Figure 8), under uniaxial compression, the curve still exhibited fluctuations after the stress reached its peak; in contrast, under confining pressure, the stress–strain curve dropped rapidly after reaching its peak. The failure characteristics of the coal rock transitioned from plastic failure to brittle failure.

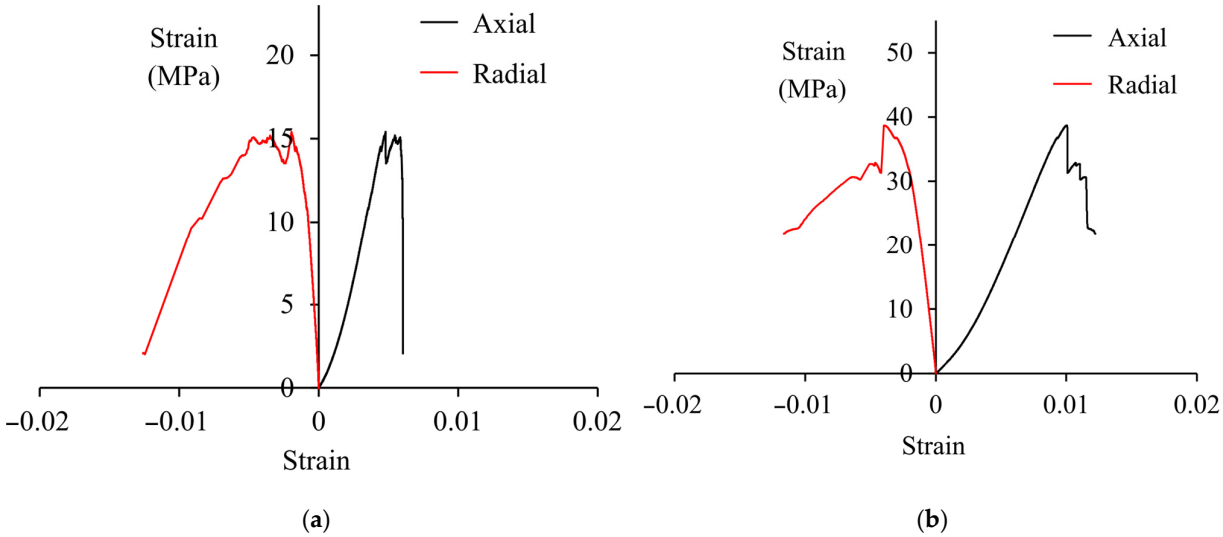


Figure 8. Coal compression stress–strain curves. (**a**) Coal C-2; (**b**) Coal C-4.

Fitting the strength versus confining pressure data from uniaxial/triaxial tests and plotting Mohr's circles (Figure 9) based on the Mohr-Coulomb criterion yielded a cohesion of 2.27 MPa and an internal friction angle of 56.80° for the coal.

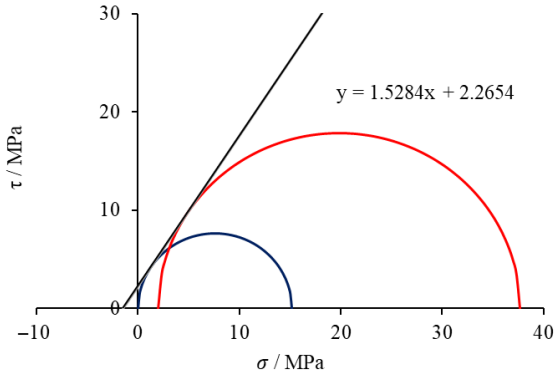


Figure 9. Coal Mohr circles.

3.5. Numerical Simulation Results

Through numerical simulation, this section investigated the influence of natural fracture density, their orientation relative to the maximum horizontal principal stress, and their individual dimensions on hydraulic fracture propagation. Based on rock mechanics test results, the coal reservoir elastic modulus was set to 4 GPa, Poisson's ratio was set to 0.3; reservoir matrix cohesion was set to 3 MPa, and internal friction angle was set to 60°.

Due to limitations in computational efficiency, the natural fracture density in the formation model was defined as the number of fractures per meter along the wellbore direction. The equivalent face cleats were modeled as rectangles with an equivalent radius of 10 m and an aspect ratio of 2.5, while the butt cleats were modeled as rectangles with an equivalent radius of 5 m and the same aspect ratio of 2.5. When investigating the influence of fracture dimension on hydraulic fractures, the equivalent radius of the face cleats was varied, while the dimensions of the butt cleats were kept constant.

Table 4 presents both the baseline parameters for the numerical model and the values adopted in the subsequent sensitivity analysis. Figure 10 depicts the naturally fractured formation model constructed using these baseline parameters.

Table 4. Numerical simulation geological and engineering parameters.

No.	Parameter	Baseline Value	Values Investigated
1	Natural fracture density (1/m)	0.3	0.1, 0.3, 0.5, 0.7
2	Angle between natural fracture and σ_H (°)	30°	0, 30, 45, 60
3	Natural fracture size (m)	10	5, 10, 15, 20

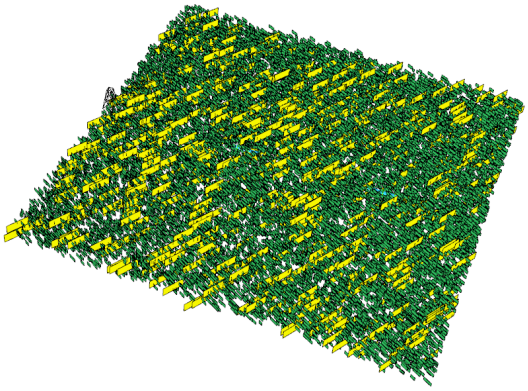


Figure 10. Numerical model of natural fracture according to baseline parameters.

3.5.1. Influence of Natural Fracture Density

As shown in Figure 11, hydraulic fracture length decreases with increasing fracture density. The SRV showed a fluctuating but generally decreasing trend. When fracture density increased from 0.1 to 0.7, hydraulic fracture length decreased by approximately 25.6%, and SRV decreased by approximately 14.8% (Figure 12).

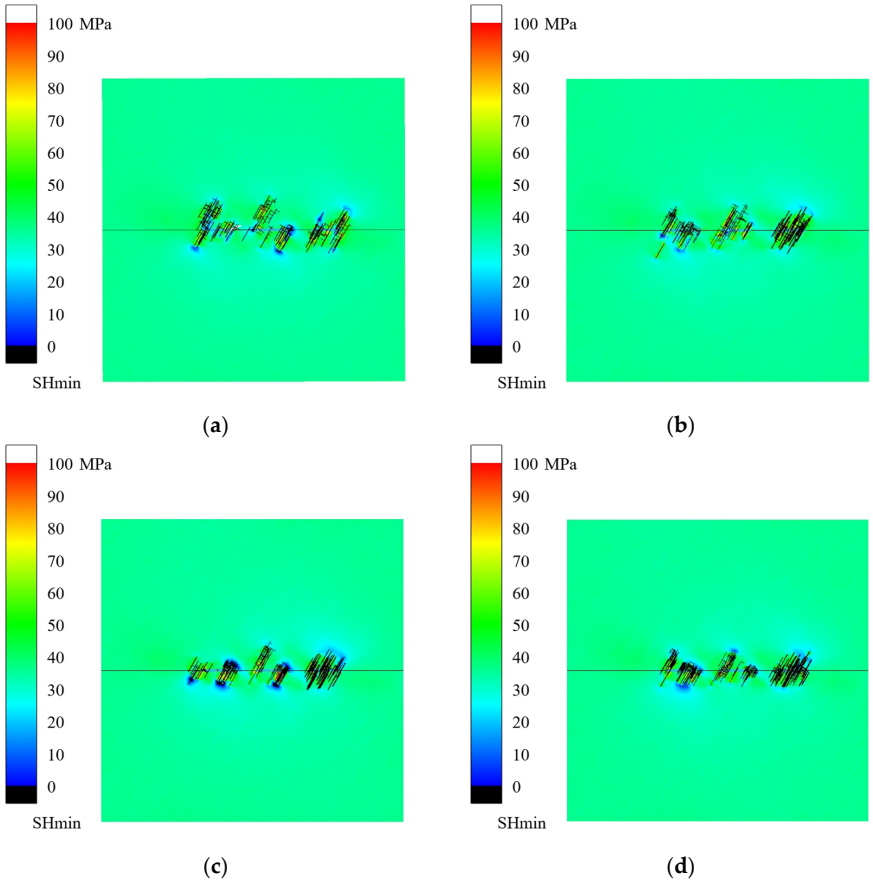


Figure 11. Hydraulic fracture networks under different natural fracture densities. (**a**) 0.1; (**b**) 0.3; (**c**) 0.5; (**d**) 0.7.

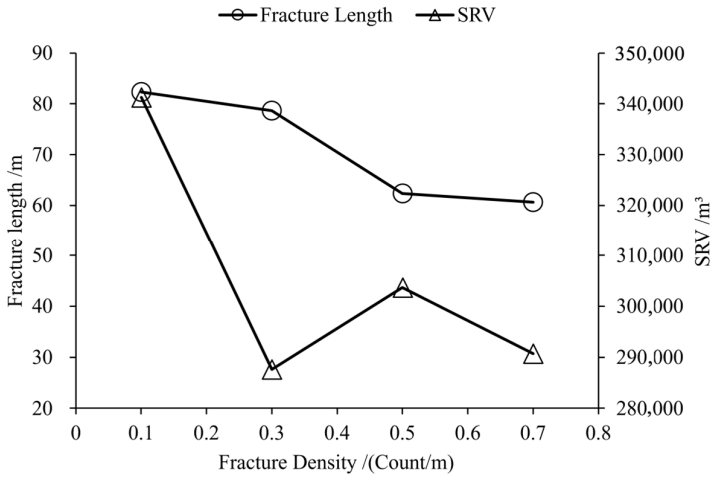


Figure 12. Hydraulic fracture length and SRV under different natural fracture densities.

3.5.2. Influence of Natural Fracture Orientation

As shown in Figure 13, varying the angle between natural fractures and the maximum principal stress (0° to 60°) showed that the farthest distance of hydraulic fractures from the wellbore gradually decreased, and the SRV also progressively declined. As shown in Figure 14, when the angle increased from 0° to 60°, hydraulic fracture length decreased by approximately 44.7%, and SRV decreased by approximately 38.8%.

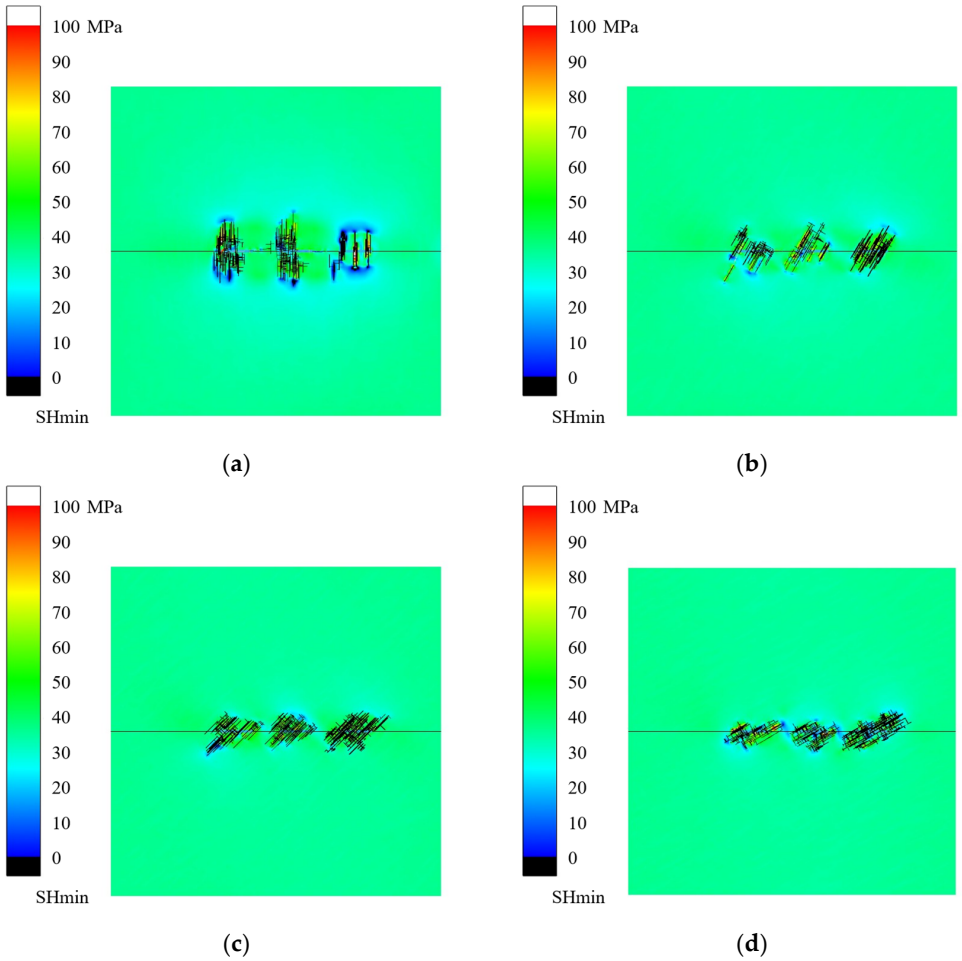


Figure 13. Hydraulic fracture networks under different fracture-stress angles. (**a**) 0°; (**b**) 30°; (**c**) 45°; (**d**) 60°.

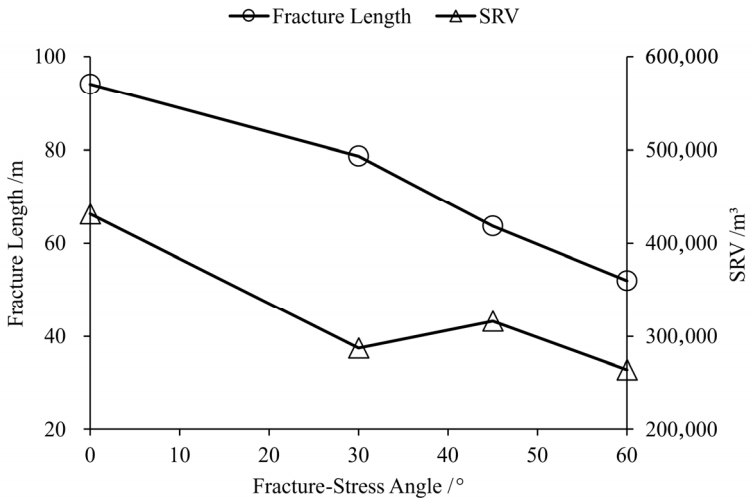


Figure 14. Hydraulic fracture length and SRV under different fracture-stress angles.

3.5.3. Influence of Natural Fracture Dimension

As shown in Figure 15, simulation results indicated a sharp drop in hydraulic fracture length when the natural fracture dimension reached 10 m, followed by a gradual decline. As shown in Figure 16, the SRV showed a similar sharp drop at the same size threshold, after which no significant further change was observed.

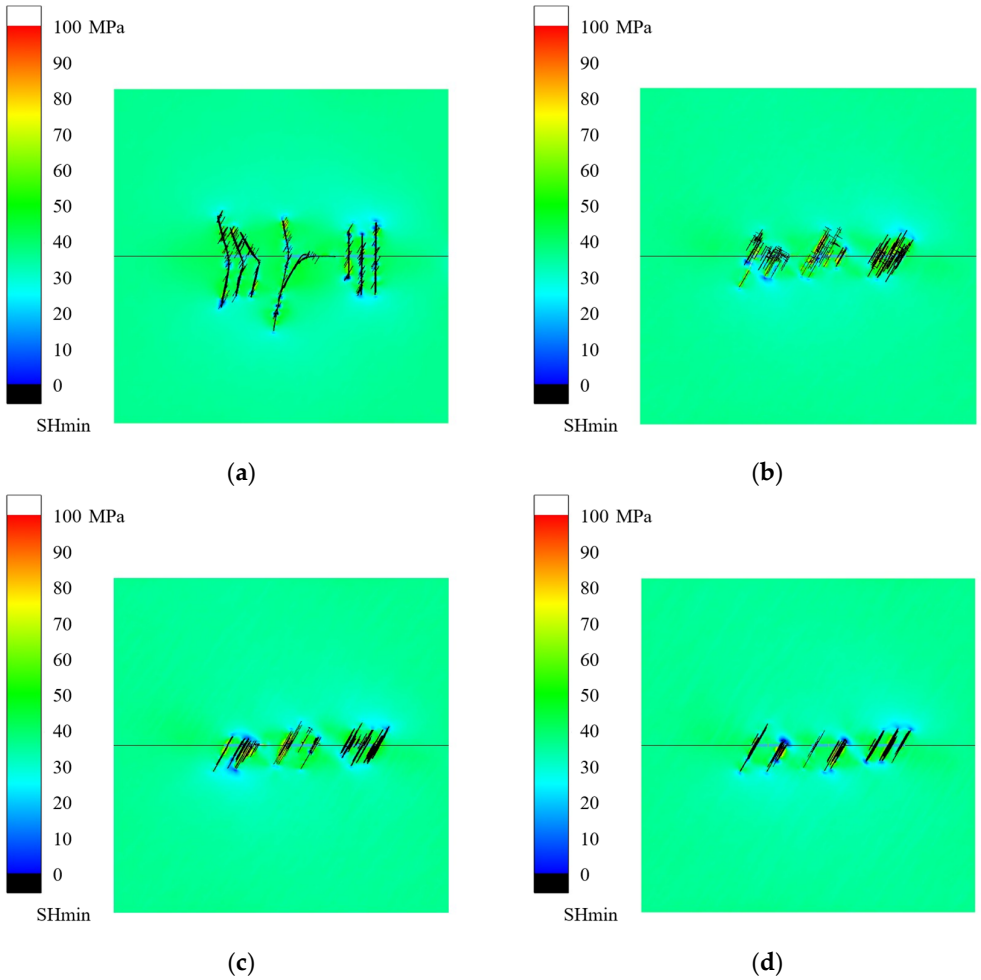


Figure 15. Hydraulic fracture networks under different natural fracture sizes. (**a**) 5 m; (**b**) 10 m; (**c**) 15 m; (**d**) 20 m.

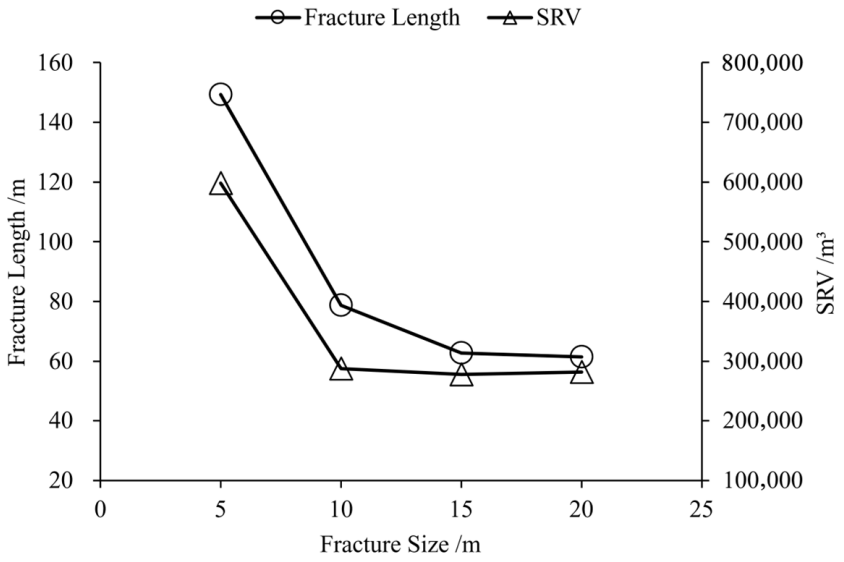


Figure 16. Hydraulic fracture length and SRV under different natural fracture sizes.

4. Discussion

4.1. Discussion of Experimental Results

CT scan results of coal revealed a complex distribution of cleats within the specimens, with the presence of approximately orthogonal cleat sets. This naturally occurring networked fracture system provides a fundamental condition for efficient CBM extraction. Under high pressure, the rock mass is prone to fragmentation along cleats, potentially leading to sand production.

The organic matter content in coal is high (80%), and nanoindentation tests demonstrated its low elastic modulus (average 4.15 GPa). Uniaxial and triaxial tests showed the elastic modulus of coal specimens to be around 4 GPa, indicating that the abundant organic matter dictates the low elastic modulus characteristic of coal. The stress–strain curves of coal exhibited fluctuations after reaching peak compressive strength, suggesting plastic behavior. It is inferred that post-failure shear sliding is inhibited by cleat surfaces, causing stress to rise again after initial failure.

The low elastic modulus of coal indicates that during hydraulic fracturing, even low net pressure can induce significant deformation, resulting in increased fracture width, which in turn leads to greater fracturing fluid consumption.

4.2. Numerical Simulation and Discussion

When conducting hydraulic fracturing in coal reservoirs with developed natural fractures, the influence of these fractures must be carefully considered. The complex cleat system exerts a complicated influence on hydraulic fracture propagation. Increased natural fracture density leads to significant fluid consumption near the wellbore, inhibiting the extension of hydraulic fractures to the far field. Unlike coal fracturing, in shale gas development, fracturing operations typically target areas with higher natural fracture density, or alternatively, aim to increase artificial fracture density to enhance the SRV [42].

As the angle between natural fractures and the minimum principal stress decreased, the farthest extent of the main hydraulic fractures from the wellbore shortened. However, fracture propagation length in the direction of the minimum principal stress gradually increased according to the simulation images, minimizing unstimulated areas between fractures and achieving more comprehensive stimulation. As noted by Zhao et al. [43], the cleat system in coal exerts a guiding effect on hydraulic fractures. During fracturing

operations, the angle between hydraulic fractures and the predominant orientation of natural fractures can be adjusted to achieve optimal stimulation performance.

Smaller natural fractures are more easily activated and opened by fracturing fluid. As fracture size increased, the resulting fracture network became simpler. Smaller natural fractures (like butt cleats) were less likely to be opened, leaving larger unstimulated areas between primary fractures.

While this study establishes a link between the microscopic properties of coal and hydraulic fracturing, certain limitations remain. Although the natural fracture model captures the three-dimensional orthogonal cleat system, it still assumes planar fracture surfaces. Due to equipment limitations, the confining pressure applied in the experiments was lower than the in situ stress. Furthermore, the difficulty of acquiring in situ coal specimens restricted the specimen quantities, which precludes more systematic conclusions.

4.3. Case Study Discussion

Geological and engineering conditions in the field are often more complex than those in laboratory experiments and numerical simulations. This study selected a hydraulic fracturing case from a coal reservoir at approximately 2000 m depth on the eastern margin of the Ordos Basin. Reservoir pressure was 29 MPa, with a horizontal stress difference of 5 MPa. Fracturing fluid volume was 4092 m^3 injected at 18 m^3/min. The fracturing stage was 60 m long with two clusters. A pump-off/flowback diversion technique was employed during fracturing. As shown in Figure 17, the treatment curve showed a significant pressure increase after a 90 min shut-in compared to the previous stage, indicating the opening of new fractures. The micro-seismic monitoring results show that after the re-pumping, the number of distant fractures significantly increased. Furthermore, isolated micro-earthquake (Figure 18) events were observed, indicating that hydraulic pressure had altered the original stress field, and that natural fractures were activated without the direct effect of fluid pressure.

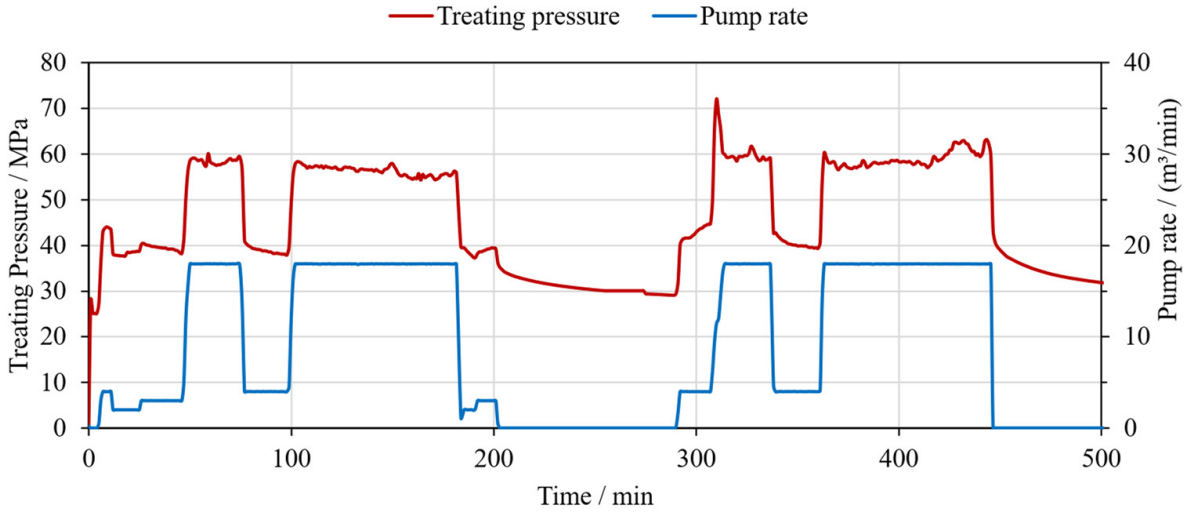


Figure 17. Treatment pressure and pumping rate curve for coal reservoir fracturing.

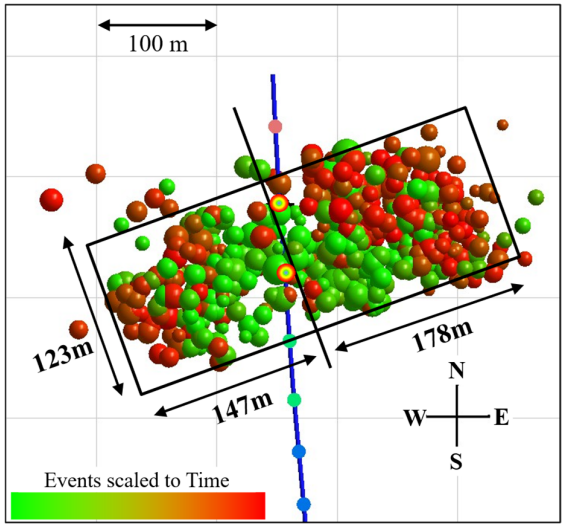


Figure 18. Micro-seismic monitoring interpretation results.

To address the challenges of limited far-field fracture propagation and small SRV during hydraulic fracturing in deep coalbed methane reservoirs, incorporating a pump shutdown during the treatment can promote fracture extension into unstimulated regions by leveraging changes in the stress field.

5. Conclusions

This study analyzed the characteristics of natural fractures in coal and their influence on hydraulic fracture propagation in coal formation through experimental testing and numerical simulation. It was found that dense natural fractures and low elastic modulus of coal reservoirs hinder the extension of hydraulic fractures to the far field in the near-wellbore region. In hydraulic fracturing design, cluster spacing can be optimized based on natural fracture density, and the angle between hydraulic fractures and the natural fracture system can be optimized by adjusting perforation angles, thereby enhancing the far-field propagation capability of fractures.

Due to the difficulty of acquiring in situ coal core specimens and the limitations of laboratory scale, the number of specimens in this study is relatively small, preventing a systematic understanding of the mechanical properties of coal. The numerical simulations still simplify fractures and do not consider the influence of fluid–solid interaction on fracture propagation, which can be possibly modeled by multiphysics numerical methods [44–46]. Future research should further investigate based on fluid–solid coupling to improve the realism of simulations.

Author Contributions: Conceptualization, Y.Q.; methodology, G.R.; software, J.B.; validation, G.R.; formal analysis, H.W.; investigation, H.W.; resources, H.W.; data curation, J.B.; writing—original draft preparation, J.B.; writing—review and editing, H.W.; visualization, J.B.; supervision, Y.Q.; project administration, Y.Q.; funding acquisition, Y.Q. and G.R. All authors have read and agreed to the published version of the manuscript.

Funding: This research was funded by Oil & Gas Major Project of Ministry of Science and Technology of the People's Republic of China "Multi-scale Testing and Prediction Techniques for Complex Lithology/Structure Rock Mechanical Properties" (2025ZD1401402), and Science and Technology Project of China National Petroleum Corporation: Research on Key Technologies for the Transformation of Unconventional Reservoirs (2023ZZ28YJ02).

Institutional Review Board Statement: Not applicable.

Data Availability Statement: The original contributions presented in this study are included in the article. Further inquiries can be directed to the corresponding author.

Conflicts of Interest: All authors were employed by the company CNPC Engineering Technology R&D Company Limited. The authors declare that the research was conducted in the absence of any commercial or financial relationships that could be construed as a potential conflict of interest.

Abbreviations

The following abbreviations are used in this manuscript:

CBM	Coalbed Methane
CT	Computed Tomography
DFN	Discrete Fracture Network
XRD	X-ray Diffraction
SRV	Stimulated Reservoir Volume
φ	the angle between the cleat and the vertical direction.
θ	the angle between the cleat and a fixed direction.
σ_H	Max Horizontal Stress

References

1. Li, G.; Jia, C.; Zhao, Q.; Zhou, T.; Gao, J. Coal-rock gas accumulation mechanism and the whole petroleum system of coal measures. *Pet. Explor. Dev.* **2025**, *52*, 29–43. [CrossRef]
2. Lei, Q.; Xu, Y.; Cai, B.; Guan, B.; Wang, X.; Bi, G.; Li, H.; Li, S.; Ding, B.; Fu, H.F.; et al. Progress and prospects of horizontal well fracturing technology for shale oil and gas reservoirs. *Pet. Explor. Dev.* **2022**, *49*, 166–172. [CrossRef]
3. Zou, C.; Yang, Z.; He, D.; Wei, Y.; Yang, S. Theory, technology and prospects of conventional and unconventional natural gas. *Pet. Explor. Dev.* **2018**, *45*, 575–587. [CrossRef]
4. Zhou, L.; Xiong, X.; Ding, R.; Li, Y. Connotation, enrichment mechanism and practical significance of coal-rock gas. *Nat. Gas Ind.* **2025**, *45*, 1–15.
5. Ju, Y.; Liu, P.; Chen, J.; Yang, Y.; Ranjith, P.G. CDEM-based analysis of the 3D initiation and propagation of hydrofracturing cracks in heterogeneous glutenites. *J. Nat. Gas Sci. Eng.* **2016**, *35*, 614–623. [CrossRef]
6. Li, Z.Q.; Li, X.L.; Yu, J.B.; Cao, W.D.; Wang, X.H. Influence of existing natural fractures and beddings on the formation of fracture network during hydraulic fracturing based on the extended finite element method. *Geomech. Geophys. Geo-Energy Geo-Resour.* **2020**, *6*, 58. [CrossRef]
7. Maxwell, S.C.; Urbancic, T.J.; Steinsberger, N.; Zinno, R. Microseismic imaging of hydraulic fracture complexity in the Barnett shale. In *Paper 77440, Presented at the SPE Annual Technical Conference and Exhibition, San Antonio, TX, USA, 29 September–2 October 2002*; SPE: New York, NY, USA, 2002.
8. Lyu, S.; Wang, S.; Chen, X.; Wang, S.; Wang, T.; Shi, X.; Dong, Q.; Li, J. Natural fractures in soft coal seams and their effect on hydraulic fracture propagation: A field study. *J. Pet. Sci. Eng.* **2020**, *192*, 107255. [CrossRef]
9. Cheng, Y.; Lu, Y.; Ge, Z.; Liang, C.; Zhang, W. Experimental study on crack propagation control and mechanism analysis of directional hydraulic fracturing. *Fuel* **2018**, *218*, 316–324. [CrossRef]
10. Jiang, T.; Haiwang, Y.E.; Ren, G.; Zhang, J.; Li, Y.B.; Wang, J.; Hao, W.; Zhang, C.; Huang, G.; Bo, K. Crack initiation and propagation in coalbed gas reservoir during hydraulic fracturing. *Sadhana* **2019**, *44*, 43. [CrossRef]
11. Wu, J.; Zhang, S.; Cao, H.; Zheng, M.M.; Qu, F.L.; Peng, C.W. Experimental investigation of crack dynamic evolution induced by pulsating hydraulic fracturing in coalbed methane reservoir. *J. Nat. Gas Sci. Eng.* **2020**, *75*, 103159. [CrossRef]
12. Huang, B.; Chen, S.; Zhao, X. Hydraulic fracturing stress transfer methods to control the strong strata behaviours in gob-side gateroads of longwall mines. *Arab. J. Geosci.* **2017**, *10*, 236. [CrossRef]
13. Ai, C.; Li, X.X.; Zhang, J.; Jia, D.; Tan, W.J. Experimental investigation of propagation mechanisms and fracture morphology for coalbed methane reservoirs. *Pet. Sci.* **2018**, *15*, 815–829. [CrossRef]
14. Bai, J.; Wang, H.; Qiao, Y.; Gong, W.X.; Zhang, Y.; Zu, K. Research on the influencing rule and main controlling factor coalbed methane reservoir stimulation. In *Proceedings of the 59th U.S. Rock Mechanics/Geomechanics Symposium, Santa Fe, NM, USA, 8–11 June 2025*; American Rock Mechanics Association: Westminster, CO, USA, 2025.
15. Ren, Q.; Zhao, Y.; Zhu, X.; Zhou, Y.; Jiang, Y.; Wang, P.; Zhang, C. CDEM-based simulation of the 3D propagation of hydraulic fractures in heterogeneous Coalbed Methane reservoirs. *Comput. Geotech.* **2022**, *152*, 104992. [CrossRef]
16. Tan, P.; Jin, Y.; Han, K.; Zheng, X.; Hou, B.; Gao, J.; Chen, M.; Zhang, Y. Vertical propagation behavior of hydraulic fractures in coal measure strata based on true triaxial experiment. *J. Pet. Sci. Eng.* **2017**, *158*, 398–407. [CrossRef]

17. Huang, L.; Li, B.; Wang, B. Effects of coal bedding dip angle on hydraulic fracturing crack propagation. *Geomech. Geophys. Geo-Energy Geo-Resour.* **2023**, *9*, 30. [CrossRef]
18. Fan, T.G.; Zhang, G.Q. Influence of injection rate and fracturing fluid viscosity on hydraulic fracture geometry in coal. *J. China Univ. Pet. (Ed. Nat. Sci.)* **2014**, *38*, 117–123. [CrossRef]
19. Jiang, Y.; Liang, W.; Cai, T.; Zhang, X.; Yan, J.; Yue, S. Fracture growth and acoustic emission response in natural coal-rock blocks with different stress, fracturing medium and injection rates. *J. Pet. Sci. Eng.* **2022**, *220*, 111228. [CrossRef]
20. Li, X.G.; He, Y.T.; Yang, Z.Z.; Zhang, P.; Song, R.; Cheng, L. Numerical simulation of hydraulic fractures propagation in multiple thin coal seams. *J. China Coal Soc.* **2018**, *43*, 1669–1676. [CrossRef]
21. Teufel, L.W.; Clark, J.A. Hydraulic fracture propagation in layered rock: Experimental studies of fracture containment. *SPE J.* **1985**, *24*, 19–32. [CrossRef]
22. Wu, P.F.; Liang, W.G.; Lian, H.J.; Jiang, Y.; Geng, Y.; Cao, M. Mechanism and experimental investigation of the formation of hydro-fracture system by fracturing through the interface of large-size coal-rock. *J China Coal Soc.* **2018**, *43*, 1381–1389. [CrossRef]
23. Liu, S.; Zou, Y.; Ma, W.; Zhang, S.; Wang, X.; Han, M.; Gao, B. Fracture morphology of variable pumping-rate hydraulic fracturing in middle and deep coal reservoirs. *Pet. Explor. Dev.* **2025**, *52*, 1460–1471. [CrossRef]
24. Yang, R.; Lu, M.; Li, A.; Cheng, H.; Jing, M.; Huang, Z.; Li, G.S. Fracture propagation and fatigue damage mechanisms in pulse hydraulic fracturing of deep coal. *Pet. Explor. Dev.* **2025**, *52*, 1074–1085. [CrossRef]
25. Wang, K.; Fu, Q.; Xu, C.; Ai, Z.; Li, D.; Shu, L. The strength characteristics and competitive failure mechanism of primary coal-rock combination considering interface damage quantity. *Fuel* **2023**, *352*, 129057. [CrossRef]
26. Xu, C.; Wang, W.; Wang, K.; Hu, K.; Cao, Z.; Zhang, Y. Influence of coal-rock interface inclination on the damage and failure law of original coal-rock combination. *Eng. Fail. Anal.* **2024**, *161*, 108275. [CrossRef]
27. Ju, Y.; Xi, C.; Zhang, Y.; Mao, L.; Gao, F.; Xie, H. Laboratory in Situ CT Observation of the Evolution of 3D Fracture Networks in Coal Subjected to Confining Pressuresand Axial Compressive Loads: A Novel Approach. *Rock Mech. Rock Eng.* **2018**, *51*, 3361–3375. [CrossRef]
28. Wang, Y.; Li, X.; Wang, J.B.; Zheng, F.; Zhang, B.; Zhao, Z.H. Numerical modeling of stress Shadow effect on hydraulic fracturing. *Nat. Gas. Geosci.* **2015**, *26*, 1941–1950. [CrossRef]
29. Xia, L.; Zeng, Y.W. Stress shadow effect of alternative fracturing based on numerical simulation of PFC2D. *Rock Soil Mech.* **2018**, *39*, 4269–4277+4286. [CrossRef]
30. Tian, Z.; Xiong, Z.; Wei, Y.; Ma, S.; Hu, X. Numerical simulation of fracture propagation in deep coal seam reservoirs. *Energy Sci. Eng.* **2023**, *11*, 3559–3574. [CrossRef]
31. Xu, W.; Zhao, J.; Rahman, S.S.; Li, Y.; Yuan, Y. A comprehensive model of a hydraulic fracture interacting with a natural fracture: Analytical and numerical solution. *Rock Mech. Rock Eng.* **2019**, *52*, 1095–1113. [CrossRef]
32. Dahi-Taleghani, A.; Olson, J.E. Numerical Modeling of Multistranded-Hydraulic-Fracture Propagation: Accounting for the Interaction Between Induced and Natural Fractures. *SPE J.* **2011**, *16*, 575–581. [CrossRef]
33. Liu, J.; Yi, L.; Yang, Z.; Yi, D.; Li, X.; Fang, J. An adaptive multiscale cohesive phase-field method for hydraulic fracturing in cleat-developed coal seams. *Comput. Geotech.* **2026**, *192*, 107890. [CrossRef]
34. Wang, W.; Jiang, L.; Wen, Z.; Zhao, Y.; Gao, M.T.; Yang, X. Dominant fracture size and equivalent DFN modeling for coal-rock mass: A discrete element study based on CT scanning. *Green Smart Min. Eng.* **2026**, *3*, 65–78. [CrossRef]
35. Jin, Z.; Hou, X.; Ge, Y.; Guo, T.K.; Chen, M.; Li, S.Y.; Niu, T.Y. Numerical Simulation of Cross-Layer Propagation Mechanisms for Hydraulic Fractures in Deep Coal-Rock Formations. *Energy Eng.* **2026**, *123*, 16. [CrossRef]
36. Song, S.; Li, L.; He, S.; Xue, Y.; Pan, H.; Bao, R.; Cao, X.; Liu, G. Quantitative characterization of fractal features of coal rock pore-fracture based on ResUnet-CBAM modeling. *Measurement* **2026**, *267*, 120609. [CrossRef]
37. Lu, J.; Jiang, W.; Xie, H.; Gao, H.; Zhang, D. Dynamic disaster mechanism and acoustic emission evolution of deep coal-rock under true triaxial disturbance stress. *J. Rock Mech. Geotech. Eng.* **2025**, *17*, 5829–5844. [CrossRef]
38. Lu, H.; Xia, C.; Xu, C.; Wang, C.; Zhao, H.; Maruvanchery, V.; Li, G. Precursory characteristics of coal-rock failure using acoustic emission and computed tomography under uniaxial monotonic and cyclic compression. *Measurement* **2025**, *247*, 116844. [CrossRef]
39. Park, J.Y.; Kim, Y.; Lee, S.; Lim, J. X-ray beam-position feedback system with easy-to-use beam-position monitor. *J. Synchrotron Radiat.* **2018**, *25*, 869–873. [CrossRef]
40. Zhang, Z.-X.; Ge, H.-K.; Wang, J.-B.; Liu, J.T.; Liu, D.; Teng, W.; Shen, Y. Influence of gravel content and cement on conglomerate fracture. *Pet. Sci.* **2023**, *20*, 1724–1741. [CrossRef]
41. Oliver, W.C.; Pharr, G.M.J. An Improved Technique for Determining Hardness and Elastic Modulus Using Load and Displacement Sensing Indentation Experiments. *J. Mater. Res.* **1992**, *7*, 1564. [CrossRef]
42. Chang, X.; Teng, S.; Wang, X.; Guo, Y.; Yang, C. Enhancing uniformity of multi-fracture propagation by temporary plugging and diversion fracturing in a horizontal well with multicluster perforations. *Pet. Sci.* **2025**, *22*, 3688–3708. [CrossRef]
43. Zhao, Z.; Wu, T.; Guo, J.; He, J.; Wen, X.; Liu, Y.; Zhang, R. Study on the spatial and temporal evolution law of large-size fracture propagation in deep coalbed based on acoustic emission technology. *Rock Mech. Rock Eng.* **2025**, *58*, 3799–3814. [CrossRef]

44. Yang, C.; Zhao, J.; Zhu, F. Coupled thermo-hydrodynamic-mechanical peridynamics for thermal fluid-solid interactions with fracturing. *J. Mech. Phys. Solids* **2026**, *208*, 106492. [CrossRef]
45. Yang, C.; Zhu, F.; Zhao, J. A multi-horizon fully coupled thermo-mechanical peridynamics. *J. Mech. Phys. Solids* **2024**, *191*, 105758. [CrossRef]
46. Yang, C.; Zhu, F.; Zhao, J. Coupled total- and semi-Lagrangian peridynamics for modelling fluid-driven fracturing in solids. *Comput. Methods Appl. Mech. Eng.* **2024**, *419*, 116580. [CrossRef]

Disclaimer/Publisher's Note: The statements, opinions and data contained in all publications are solely those of the individual author(s) and contributor(s) and not of MDPI and/or the editor(s). MDPI and/or the editor(s) disclaim responsibility for any injury to people or property resulting from any ideas, methods, instructions or products referred to in the content.